Skin Cooling of Turbine Airfoils by Single-Wall Effusion—Part II: Computational Fluid Dynamics Validation and Preliminary Design Optimization on a Micro-Turbine Vane

Yair Lange
Faculty of Aerospace Engineering,
Turbo & Jet Engine Laboratory,
Technion – Israel Institute of Technology,
Haifa 32000, Israel
e-mail: ylange@alumni.technion.ac.il

S. Fatih Kırmızıgöl
Faculty of Engineering and Architecture,
Mechanical Engineering Laboratory,
İzmir Katip çelebi University,
İzmir 35620, Turkey
e-mail: fatihk@esalba.com

Sercan Acarer
Associate Professor of Mechanical Engineering
Faculty of Engineering and Architecture,
Mechanical Engineering Laboratory,
İzmir Katip çelebi University,
İzmir 35620, Turkey
e-mail: sercan.acarer@ikcu.edu.tr

Beni Cukurel[1]
Mem. ASME
Associate Professor of Aerospace Engineering
Faculty of Aerospace Engineering,
Turbo & Jet Engine Laboratory,
Technion – Israel Institute of Technology,
Haifa 32000, Israel
e-mails: bcukurel@technion.ac.il;
beni@cukurel.org

A reduced-order model (ROM) is developed to capture conjugate aero-thermal physics of effusion cooling in an entire micro-turbine vane/blade. The model considers a single-wall effusion scheme with internal boundary layer flow between the shell and an inner core. Coolant is supplied inside the leading edge and spread to both suction and pressure sides. The compound effect of multiple effusion rows is used to calculate spanwise-averaged cooling effectiveness. Metal temperature is modeled both in streamwise and shell thickness directions. The development of the model and a number of numerical/experimental validation cases are presented in detail in Part I. Part II of the work is geared toward the application of this method to skin cooling of a turbine airfoil by single-wall effusion. The reduced-order model, with all its subroutines functioning together, is validated against a higher fidelity 3D Reynolds-averaged Navier–Stokes (RANS) computational fluid dynamics (CFD) solution. It is shown that the model can predict the main features of the combined internal and effusion cooling in gas-turbine blades at a computational cost which is 10^5 times lower than RANS (~1 month with 700M elements and 24 modern Xeon Cores) on a whole turbine vane/blade. Due to this great advantage in speed, a design optimization is then accomplished toward minimizing coolant flow rate while keeping thermal gradients and temperature of the solid within acceptable levels. Implementing this scheme on a typical micro-gas-turbine vane, optimal distributions of the effusion-hole pitch and diameter are found within a given set of constraints. This preliminary design tool potentially enables wider and more efficient usage of effusion cooling in turbine vanes/blades.
[DOI: 10.1115/1.4056877]

Keywords: effusion cooling, skin cooling, design optimization, micro-gas turbines, preliminary design tool, reduced-order model, aerospace heat transfer, porous media, thermal systems

Introduction

Achieving higher gas turbine performance through augmentation of turbine inlet temperature (TIT) has been pursued both for propulsion and power generation. Raising TIT enables a higher thrust/weight ratio and allows the operation of the thermodynamic cycle in higher compressor pressure ratios that in turn yield efficiency augmentation. Therefore, there is an ever-growing demand for better turbine cooling techniques to prevent the blades from reaching their structural limits. Along these lines, there is a recent trend toward implementing micro-cooling technologies on turbine airfoils [1]. By generating a targeted thin layer over the entire surface, the optimal implementation of the technique enables reaching high and uniform effectiveness that reduces the heat load and the thermal gradients, while consuming less coolant.

Micro-Cooling Technologies Based on Film Cooling. Figure 1 shows some of the prominent micro-external cooling technologies based on film cooling. As depicted, a greater number of smaller holes define the basic difference between the film (Fig. 1(*a*)) and the effusion (Fig. 1(*b*)) cooling. At the extreme, closely packed infinitesimal holes generate a porous wall, typically referred as a transpiration cooling (Fig. 1(*c*)). Full hole coverage and high internal convective heat transfer are the beneficial features of this scheme [2]. Therefore, it has received considerable attention and simplified models have been developed for several applications [3,4]. More recently, several wall constructions are designed to mimic porous walls of transpiration cooling by creating labyrinth flow paths that increase the internally wetted surface. Comprising of inner shells, internal staggered fins (pedestals), impingement holes, and an outer shell equipped with effusion holes, Lamilloy (Fig. 1(*d*)) and Transply (Fig. 1(*e*), also called double-wall effusion cooling (EC) scheme) are engineering solutions that effectively approach transpiration cooling [5] (Lamilloy mainly differs from the Transply in having an intermediate shell between inner and outer shells).

However, only a limited number of effusion cooling studies focused on the application of the technology on turbine blades [6]. One of such studies recently published is on the effects of strong streamwise pressure gradients on the Transply scheme (Fig. 1(*e*)) applied on a flat plate by external contraction. It is experimentally revealed that relaminarization by the streamwise acceleration causes both heat transfer coefficient and film cooling

[1]Corresponding author.

Manuscript received August 3, 2022; final manuscript received January 17, 2023; published online March 31, 2023. Assoc. Editor: Lesley Wright.

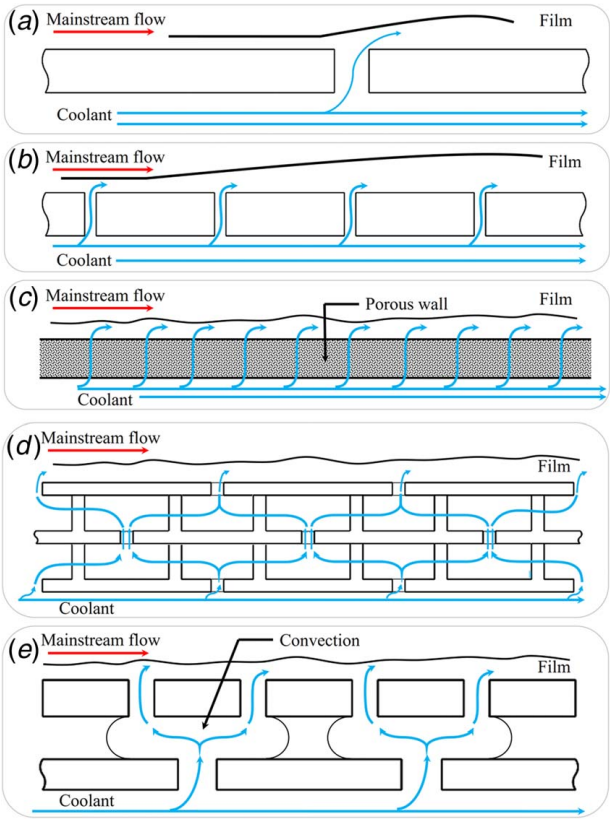

Fig. 1 Some prominent film cooling schemes: (*a*) conventional film cooling, (*b*) single-wall effusion cooling, (*c*) transpiration cooling, (*d*) Lamilloy, and (*e*) Transply (double-wall effusion cooling). Figure redrawn from Ref. [5].

effectiveness to drop at streamwise locations larger than 60 times the hole diameter in case the initial (first hole) blowing ratio is fixed [7]. Another very recent experimental study considered full blade transpiration and effusion cooling schemes over an isolated airfoil in a subsonic wind tunnel [8]. It is shown that if high blowing ratios cannot be prevented (e.g., with a porous media at coolant supply), effusion cooling may be adversely affected, even performing less effectively than the internal cooling scheme alone. This was not observed for the transpiration cooling.

On the numerical side, most studies focus on cost-effective modeling that includes aero-thermal coupling (so-called "decoupled conjugate method" [9,10]), originally developed to predict thermal stresses for the Transply scheme. It considers modified Goldstein correlations [11] for film cooling effectiveness that includes streamwise decay. Sellers model [12] was implemented and validated [13] for compound cooling associated with multiple holes in 2D. A conjugate computational fluid dynamics (CFD) simulation with simplified boundary conditions on a small periodic model predicted the internal fluid flow. The obtained internal heat transfer coefficient field was replicated on the larger geometry utilized in thermomechanical computations. A 3D conduction model uses these data to calculate the thermal profile required for thermomechanical simulations. Such an approach was shown to decrease simulation time as much as two orders of magnitude with reasonable accuracy [14].

In a more recent study, Elmukashfi et al. [15] developed an even further simplified 2D thermomechanical numerical model for the same problem. The geometry is simplified to form an axisymmetric 2D model centered on one of the pedestals. A combination of empirical correlations and profiles, approximately scaled from prior CFD simulations on some representative cases, is used to define the boundary conditions. The method provides rapid thermal stress predictions; however, the accuracy and the range of design space are limited due to the simplifications and assumptions involved.

Similarly, Murray et al. [16] recently developed a 1D algebraic reduced-order model (ROM) in order to predict aero-thermal performance of a similar Transply scheme. It employs thermal resistance circuit analogy and considers major elements of aero-thermal processes occurring in Transply scheme. Compilation of several relevant empirical correlations supplies the required thermal resistances. A combination of experimental and computational data on four different representative geometries validated the model with success. The results indicate that the model can be used to optimize aero-thermal response of such a complex problem rapidly with high accuracy.

A significant challenge for implementing micro-cooling technologies is achieving an optimal coolant air distribution across the blade surface, driven by a varying heat flux load from the external flow. Cerri et al. [5] reported one of the very few works in open literature that deals with the optimization of the effusion cooling hole diameter and pitch distribution in a hollow airfoil geometry. Assuming constant blade temperature and maximum blowing ratio, the through flow in the airfoil skin was modeled and optimization was geared toward manufacturability concerns. However, this numerical framework was absent of external or internal flow considerations and neglected conduction effects across the airfoil material.

Motivation. There have been recent developments in the literature on cost-effective conjugate modeling of double-wall effusion cooling schemes and their application to the turbine blade environment. However, to the authors' best knowledge, a conjugate ROM that predicts the performance of the single-wall effusion cooling scheme (described in Fig. 1(*b*)) in turbine applications does not exist, which is a simple and strong alternative to double-wall cooling systems for small-scale turbines and more research is needed in this area. Part I of this paper attempts to fill this void by developing a set of equations, their solution algorithm, and validation.

Due to the disparity of geometric scales with feature size as small as 50 μm, the CPU time of a conjugate heat transfer (CHT) Reynolds-averaged Navier–Stokes (RANS) CFD simulation with effusion cooling (with approximately requiring 700 million mesh elements) on a whole turbine blade/vane would approximately take ~1 month on a typical workstation (24 modern Xeon cores); and therefore, this type of approach is inhibitive for optimization and preliminary design. On the contrary, it is shown in this part that the developed ROM is suitable for parametric studies of single-wall effusion turbine cooling such that comparative accuracy is obtained at a computational time 10^5 times lower than CFD on a whole turbine vane/blade.

Along these lines, Part II demonstrates an application of this reduced-order model as a comprehensive preliminary design tool for effusion holes in skin-cooled turbines that include internal, through, and external flow considerations, as well as quasi-2D conduction in the metal. Although the presented method is expected to be valid for a broad range of conditions, the demonstrative test case is applied to a ~¼ scale NASA C3X airfoil [17], representing environments typical in micro-gas-turbine applications. A short discussion on manufacturing of such an effusion-cooled micro-turbine airfoil is also included.

Establishing Heat Load of External Flow on Uncooled Turbine Geometry

The function of any external cooling scheme is to reduce the surface temperatures homogenously against the heat load generated by external flow. Therefore, this section describes the process of formulating the heat load for an *uncooled* scaled-down C3X airfoil via validated CFD, which serves as one of the main inputs for the reduced-order model.

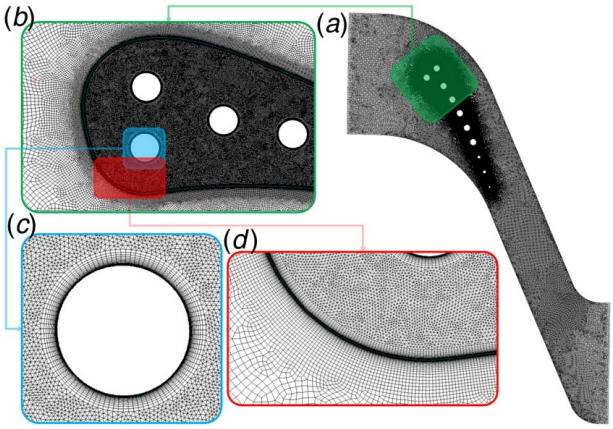

Fig. 2 CFD mesh structure of NASA C3X blade: (*a*) general depiction of grid, (*b*) detailed view of leading-edge region, (*c*) cooling channel mesh structure including inflation layers, and (*d*) outer wall adjacent boundary layer mesh

Turbulence Model Selection and Validation. In order to have external aero-thermal turbine flow representing physical phenomena, 2D RANS simulations with different turbulence closures are conducted in ANSYS Fluent 19.1 and validated against established test cases. One of the well-known experimental benchmarks is the NASA C3X turbine geometry [17], for which aerodynamic and heat transfer data are available. The geometrical details of the ASTM 310 stainless steel airfoil with 144.93 mm chord length are given in Ref. [17], where 10 internal cooling passages exist. Positioned at a stagger angle of 59.9 deg, with an axial chord-to-pitch ratio of 0.66, the transonic flow over the surface of the blade is exemplary to modern turbine airfoils.

The experimental domain is replicated in the computation, wherein a translational periodic domain is created, and the corresponding grid consisting of $\sim 2.5\ 10^5$ elements is shown in Fig. 2(*a*). A detailed view of the leading edge region is shown in Fig. 2(*b*), whereas Fig. 2(*c*) shows the mesh structure, including the inflation layers, around the cooling channels. Lastly, Fig. 2(*d*) portrays the mesh structure adjacent to the metal outer wall. The near-wall cell $y+$ value does not exceed 0.36, and the boundary layer mesh smoothly grows at a rate of 1.2, enabling modeling of the aerodynamics and convection heat transfer within reasonable accuracy. It has been observed that further mesh refinement does not affect the results.

The boundary conditions considered are identical to the experimental run 158 in the report [17]; compiled in Table 1, they are used as the reference operating point throughout this study. The inlet turbulence level is 8.3%, and the blade exit Mach number is transonic at a value of 0.9 (subscripts represent inlet (1) and outlet (2)). The internal channel heat transfer coefficients and coolant temperatures are specified according to the data provided in Ref. [18]. The resultant heat balance provides an average wall temperature of $T_w/T_r = 0.73$.

In the current CFD framework, five different turbulence closures are considered: k–ω–SST, k–ε–ML–Realizable, RSM–ω LR, Realizable k–ε and Transition–SST. The resulting static pressure (normalized with respect to $P_r = 243.7$ kPa), heat transfer coefficient (computed using 808 K as the reference temperature and normalized with respect to $H_r = 1135\ \mathrm{W\,m^{-2}\,K^{-1}}$), and wall temperature distributions (normalized with respect to $T_r = 811$ K same as in Ref. [17]) are contrasted with experimental data in Fig. 3. The spatial distribution is charted as a function of normalized streamwise direction (x/arc, where the "arc" length is the curvilinear length of pressure or suction sides from the leading edge to the trailing edge), and the orientation is such that pressure and suction sides are represented by negative and positive values, respectively.

Table 1 Main parameters for experimental run 158 [17]

Parameter	Value	Parameter	Value
P_{T_1} (kPa)	243.7	Re_1	$0.38 \cdot 10^6$
T_{T_1} (K)	808	P_{S_2} (kPa)	142.5
T_{U_1} (%)	8.3	M_2	0.91
M_1	0.17	Re_2	$1.47 \cdot 10^6$

Expectedly, all turbulence models capture the surface static pressure accurately, while in the suction side flow there are slight deviations past the turbine velocity peak point. The heat transfer coefficient and wall temperature predictions significantly vary depending on the closure. Many variants of k–ε and k–ω models (including near-wall low Reynolds submodels implemented in Fluent) did not provide a good match, neither in heat transfer coefficient nor in wall temperature predictions. These findings are in line with the observations in the literature, see Ref. [19]. The $k-\varepsilon$ Realizable model with Menter–Lechner near-wall treatment ($\mathrm{ML}-\varepsilon$) and Stress-omega Full Reynolds Stress Model (RSM–ω–LR) yield the best matches with the experimental data. However, there were stability issues experienced with the RSM–ω–LR model; therefore, $ML-\varepsilon$ was selected as the turbulence closure in all CFD conducted.

External Heat Load of Scaled-Down Blade. In order to attain a geometry representative of micro-gas-turbine blades, the external profile of the C3X geometry is scaled down to 23.1% of its original size, which results in a blade chord length of 33.5 mm, and the grid is proportionally scaled down as well. This geometry is labeled scaled-C3X (SC3X).

Using the $k-\varepsilon$ Realizable model with Menter–Lechner near-wall treatment ($\mathrm{ML}-\varepsilon$), external flow RANS simulations for the uncooled blade are conducted with the aerodynamic boundary conditions indicated in Table 1 (except with a reduced Reynolds number of 87,780 due to the scaling). Following the adiabatic heat transfer calculation methodology described in Ref. [20], multiple (3) uniform heat flux levels are imposed on the blade external surface for different runs. The local adiabatic wall temperature is computed by taking the zero crossing for the linearly extrapolated local surface temperatures as a function of the imposed heat flux values. Then, the adiabatic heat transfer coefficient is calculated by taking the adiabatic wall temperature as the reference. For the uncooled scaled-C3X geometry, Fig. 4 portrays the resultant local distributions of static pressure and adiabatic heat transfer coefficient, which are to serve as aero-thermal inputs for the reduced-order model of effusion cooling.

Application of Reduced-Order Effusion Cooling Model

Applying effusion cooling to the SC3X turbine blade (according to the physical alterations), the airfoil is separated into a solid core and a shell that contains small holes along the streamwise direction, Fig. 5. Details A and B present the cooling holes through the shell, and the shell surfaces exposed to internal and external flows, respectively. The coolant is first introduced from a circular reservoir passage around the leading edge and distributed along the inner surface of the shell across the pressure and suctions sides. In order to prevent blow off on the suction side, a small (3 mm wide) porous media is introduced as a pressure drop mechanism at the leading edge (x/arc = 0.13).

The reduced-order model in this work is comprised of a CHT module, which solves the shell internal and the hole through flows, as well as conduction in the shell, and an EC module that considers the compound effectiveness on the external surface arising from the coolant buildup. The details of the model are given in Part I of this paper.

This approach is based on three major assumptions. First, the turbulence model is validated over the original C3X blade and not over

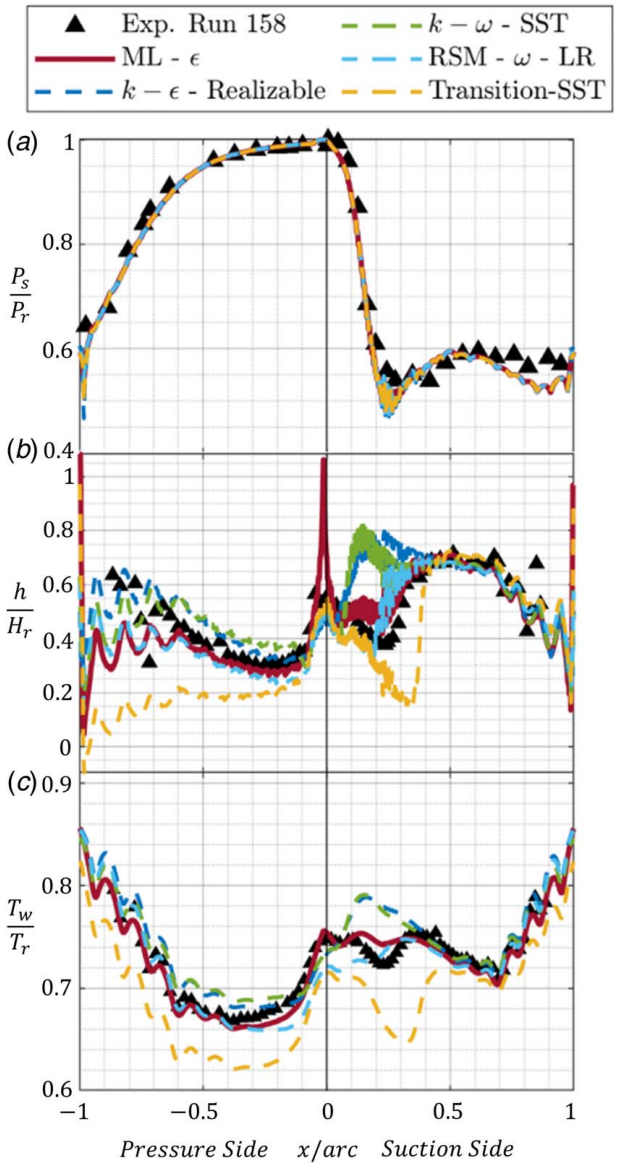

Fig. 3 Aero-thermal CFD modeling of C3X and comparison of turbulence closures with experimental data: (*a*) static pressure, (*b*) heat transfer coefficient, and (*c*) wall temperature, where $P_r = 243.7$ kPa, $H_r = 1135$ W m^{-2} K^{-1}, and T_r = 811 K

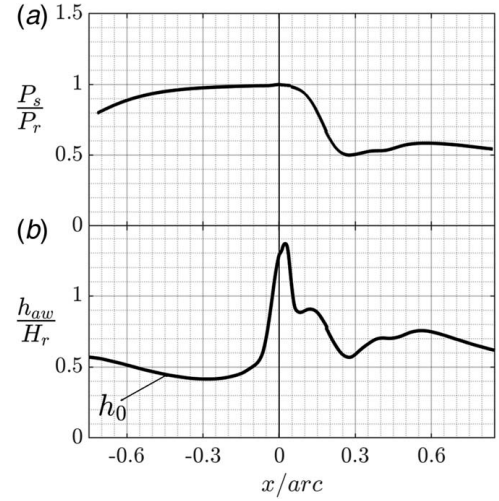

Fig. 4 Aero-thermal modeling scaled-C3X blade: (*a*) static pressure and (*b*) adiabatic heat transfer coefficient distributions, where $P_r = 243.7$ kPa and $H_r = 1135$ W m^{-2} K^{-1}

the scaled geometry, where the Reynolds number is reduced from $0.38 \cdot 10^6$ to $0.8778 \cdot 10^5$. Second, the coolant injection is assumed to not influence the static pressure distribution over the blade surface. Lastly, the dominant nondimensional parameters in the model are Reynolds number (Re), Nusselt number (Nu), Graetz number (Gz), spacing (S), effectiveness (η), blowing ratio (M), and momentum flux ratio (I).

Comparison of Reduced-Order Model to Computational Fluid Dynamics

To compare the ROM on an exemplary geometry subjected to external transonic flow, the profile of the scaled-C3X blade geometry (chord length of 33.5 mm) is used with constant diameter effusion cooling holes ($D = 0.1$ mm) at a staggered pit/$D = 10$ (where the spacing in spanwise and in streamwise directions is equal) over a shell thickness of $d_s = 0.4$ mm and internal passage height of $t = 1$ mm. The curve-linear starting point of the porous media is 6 mm and its mean length is 2.3 mm. Then, the blade is modeled by a single half pitch sector spanning 0.5 mm, with symmetric conditions specified at the two lateral ends, and periodic surfaces on the blade-to-blade plane. The combined ROM is implemented in MATLAB 2020B.

The inlet mainstream and coolant total pressures and temperatures are 243.7 kPa, 808 K and 246 kPa, 374 K, respectively, where the outlet static pressure is 142.5 kPa and the inlet turbulence intensity is 8.3%. The resultant cumulative coolant mass flowrate is 2.2% of the hot external gas path.

In order to adequately capture the film growth on the external surface, the blade exterior region is divided into two mesh domains: a fine mesh region that has normal-wall growth rate of 1.05, and a coarse region with a growth rate of 1.2. With a near-wall cell y^+ of 0.1, there are 3.8×10^7 finite volumes in total. Figure 6 shows the geometry, the computational domain, the generated mesh, and the boundary conditions.

A survey plane is created at the outlet of each hole for which the average values are probed. For the 3D CFD data and the reduced-order model, Fig. 7 shows mass flowrate, velocity, total pressure, total temperature, and effective-hole area at the exit of each hole. Findings are charted as a function of normalized streamwise directions, where negative values indicate the pressure side. Consistent with the conjugate heat transfer module validation, the hole-exit mass flowrates, velocities, temperatures, and pressures

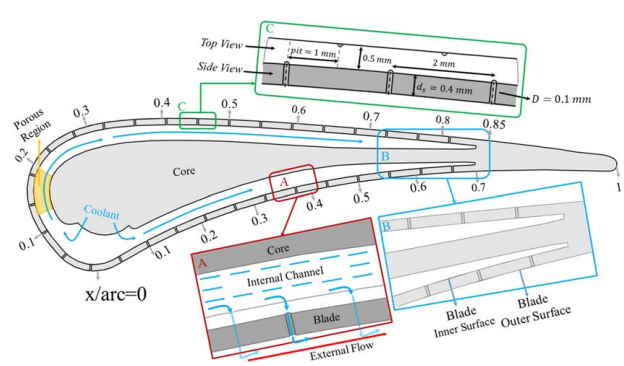

Fig. 5 2D domain of scaled-C3X blade equipped with basic effusion cooling through a solid core and a perforated shell type design, with curve-linear coordinate system indicating *x/arc* locations, and detail (A) and (B) Portray cooling holes through the shell and surfaces exposed to internal and external flows, respectively

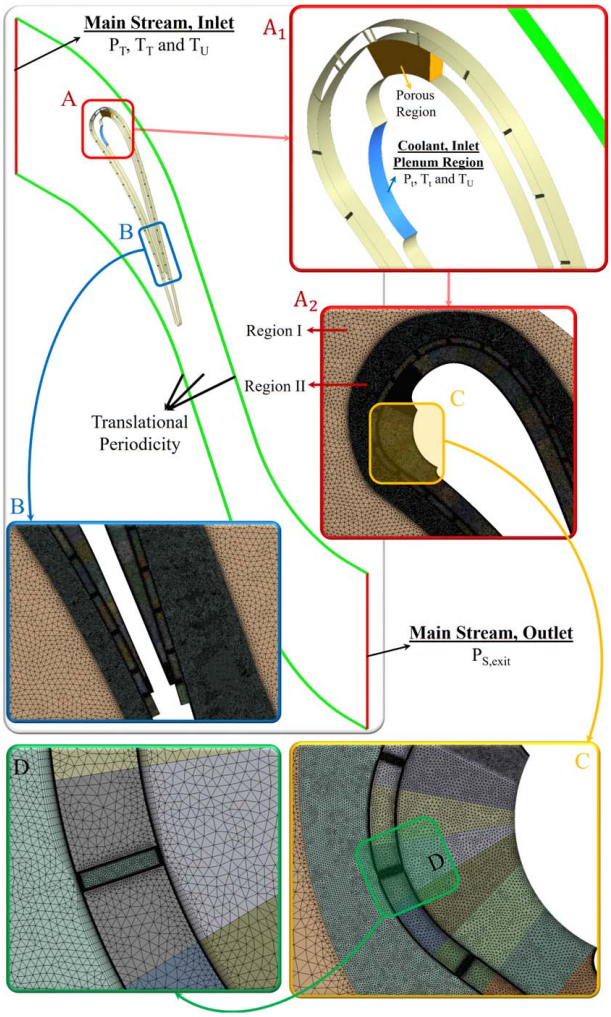

Fig. 6 Combined reduced-order model validation test case with scaled-C3X geometry sector including symmetric lateral walls and periodic blade–blade surfaces

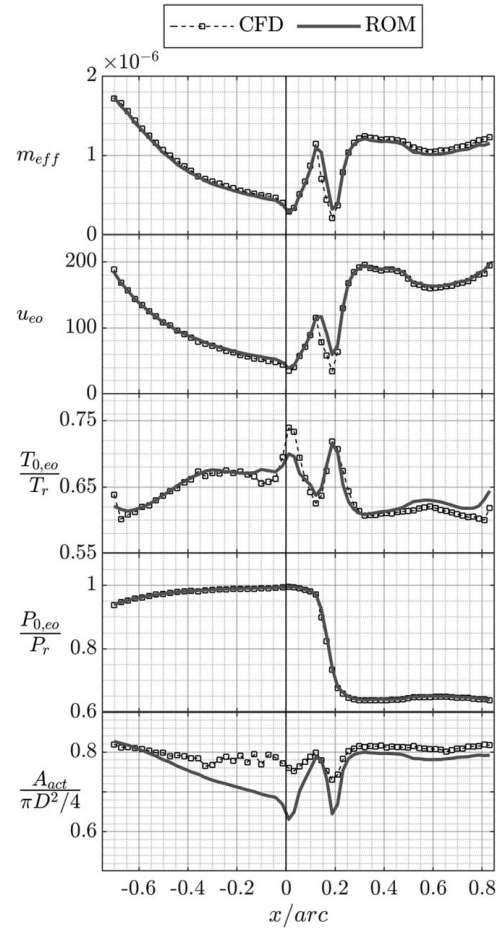

Fig. 7 Comparison of holes outlet mass flowrates, velocities, total temperatures, total pressures, and effective-hole areas between 3D CFD and the reduced-order numerical model for validation test case with scaled-C3X geometry sector (T_r = 811 K and P_r = 246 kPa)

are well predicted by the reduced-order model. Therefore, it can be deduced that densities are also well predicted. Percent error of each property is shown in Table 2. Between the CFD and the ROM, the only noticeable differences are observed in hole-exit total coolant temperatures and in effective flow area, mainly in the vicinity of the leading edge region. The local spike in CFD-predicted total temperature at the leading edge mainly stems from overprediction of turbulence (see Fig. 3) and is not directly related to ROM. The effective area is defined as the mass flowrate divided by density and velocity. Considering the highly nonuniform hole inlet flow, it is not straightforward to define this quantity consistently in CFD due to the multiplication of average velocity and density being different from the area integral of the local mass fluxes. Therefore, the observed discrepancy is a computational artifact. Additionally, Fig. 8 shows the variation of coolant flow between plenum region and internal channel region. The former is constructed from holes that face the coolant inlet, whereas the latter is constructed from holes perpendicular to the coolant flow. This geometry difference may lead to difficulty in accurately predicting effective-hole area and wall temperature in the plenum region.

Having established that the hole-exit flow is well represented in the ROM, effectiveness is computed for the CFD simulations using mass-weighted average hole-exit coolant total temperatures, adiabatic wall temperature, and the freestream total temperature. Pressure and suction side lateral and pitch-averaged effectiveness distributions are charted as a function of curve-linear coordinates, Fig. 9. Contrasting the ROM results with the CFD, the results seem to be adequately consistent for all regions, except for slight under prediction at $x/\text{arc} = -0.1$ and 0.25. These deviations might occur due to difficulty in accurately capturing the impact of potential effects associated with downstream curvature on upstream effectiveness (as mentioned in Ref. [21]).

In the ROM, the uncooled-adiabatic heat transfer coefficient h_0 is used as an input to predict the cooled-adiabatic heat transfer coefficient h_f and free stream-referenced "final" heat transfer coefficient h (see Part I of this work). These three heat transfer coefficients are charted in Fig. 9. The h_f is compared with the CFD results in the absence of conduction, acquired by changing the constant wall temperature boundary condition to levels of 520 K, 560 K, and 600 K iteratively. Overall good agreement is observed. The prediction is

Table 2 Percent error of holes outlet mass flowrates, velocities, total temperatures, total pressures, and effective-hole areas

x/arc	$\dot{m}_{eo}$%Err	u_{eo}%Err	$T_{0,eo}$%Err	$P_{0,eo}$%Err	A_{act}%Err
[−0.6, −0.4]	2.7	0.6	0.4	0.04	1.9
[−0.4, −0.2]	3.8	2.8	0.5	0.1	6.0
[−0.2, 0]	5.7	7.5	1.4	0.1	11.3
[0, 0.2]	19.0	22.5	2.5	0.7	7.1
[0.2, 0.4]	2.3	2.3	1.1	0.4	3.1
[0.4, 0.6]	3.7	1.3	1.7	0.3	2.8
[0.6, 0.8]	4.1	1.5	2.2	0.3	2.8

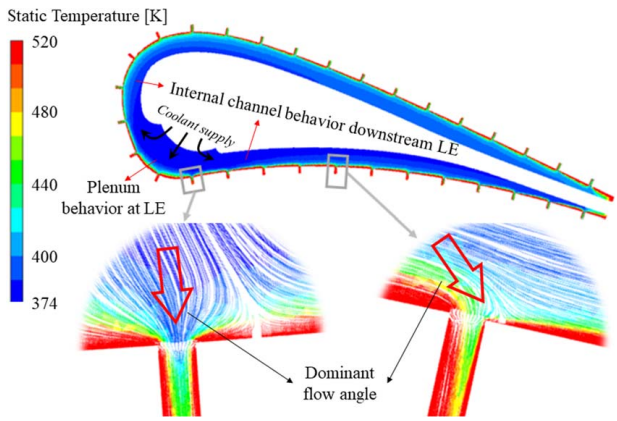

Fig. 8 Exemplary static temperature and streamline field in the vicinity of the holes: plenum behavior (left) for the regions close to the leading edge where the coolant is supplied and the internal channel behavior elsewhere (right)

not as precise near $x/\text{arc} = 0.3$ at the suction side, which can be potentially associated with the change in the location of laminar to turbulent transition. The transition location in the suction side moves slightly upstream when coolant is injected into the mainstream, in comparison to the uncooled blade. The enhancement of heat transfer is modeled through effectiveness and blowing ratio, while prediction of transition location is not addressed. Using effectiveness, h_f and the normalized coolant temperature, the freestream-referenced heat transfer coefficient h is predicted (see Part I of this work), which appears to be in good agreement with the CFD as well.

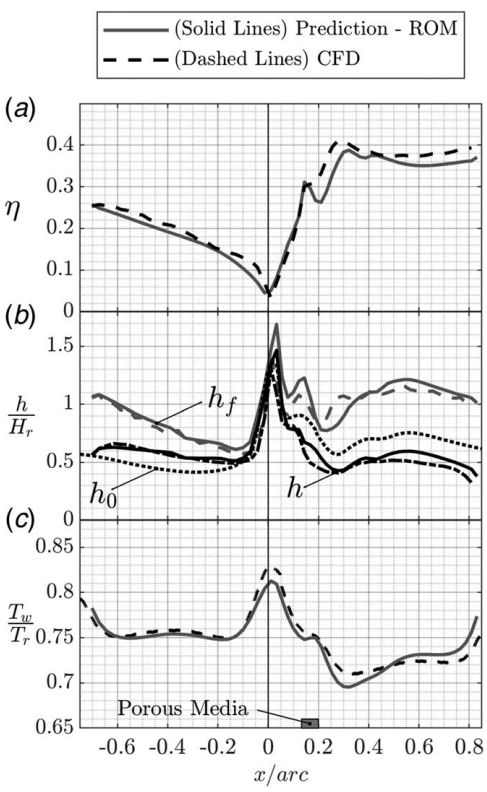

Fig. 9 Comparison of laterally and pitchwise-averaged effectiveness—η, uncooled-adiabatic heat transfer coefficient—h_0, cooled-adiabatic heat transfer coefficient—h_f, free stream-referenced heat transfer coefficient—h, and wall temperature—T_w between 3D CFD (dashed lines) and the reduced-order numerical model (solid lines) for validation test case with scaled-C3X geometry sector ($H_r = 1135$ W m^{-2} K^{-1} and $T_r = 811$ K)

Table 3 Percent error of effectiveness, cooled-adiabatic heat transfer coefficient, freestream-referenced heat transfer coefficient, and wall temperature

x/arc	η%Err	h_f %Err	h%Err	T_w%Err
[−0.6, −0.4]	8.4	4.2	3.0	0.6
[−0.4, −0.2]	7.0	3.6	4.8	0.5
[−0.2, 0]	14.2	15.2	13.2	1.5
[0, 0.2]	13.4	16.0	17.7	1.4
[0.2, 0.4]	12.4	12.2	14.8	1.8
[0.4, 0.6]	4.7	5.1	12.0	0.5
[0.6, 0.8]	6.7	5.4	15.9	1.6

While heat transfer coefficients and effectiveness distributions are calculated by the effusion cooling module, by coupling the solution with a conjugate heat transfer module, wall temperature distributions are attained. As indicated in the bottom chart of Fig. 9, while a limited localized discrepancy of 2.5% occurs at $x/\text{arc} = 0.3$ because of the error propagation from the previously mentioned inaccuracies, high general level of wall temperature agreement is achieved across the surface of the blade.

Table 3 summarizes the local efficacy of reduced-order model in capturing effectiveness, cooled-adiabatic heat transfer coefficient, freestream-referenced heat transfer coefficient, and more importantly wall temperature distributions. Considering that the prediction error is less than 17.7% across all these quantities, the presented reduced-order model seems to sufficiently capture the aero-thermal flow physics associated with internal, through, and external flow considerations, as well as the metal conduction. In terms of computational cost, on a typical computer (Intel i7 with 4 cores and 32 GB ram), the CPU time of the ROM evaluation is ~1 min, whereas the conjugate heat transfer CFD simulation takes ~100,000 min (full model for nonuniform pitch and diameter). Considering the high level of accuracy and computational cost which is 10^5 times lower than RANS, the presented reduced-order model, together with a known heat load on an uncooled blade, can serve as a preliminary design tool for effusion-cooled turbines in future developmental activity. In order to further highlight the potential benefits of this tool, an optimization exercise is demonstrated on the same section of the SC3X geometry.

Optimization

Optimization Framework. The essence of the optimization framework is to find the optimal hole diameter and hole spacing distributions in an effusion-cooled turbine toward reducing the average metal temperatures and their gradients to values below a prescribed limit, while injecting minimum coolant flow.

Therefore, the optimization outline is minimize $\dot{m}_c$ with respect to $D(x)$ and $S(x) = \text{pit}(x)/D(x)$, subject to $\max(T_w) \le T_{\max}$ and $\max(\Delta T) < (\Delta T)_{\max}$. Following this definition, the cost function (f) is formed such that the soft temperature constraints are integrated into one objective as two separate penalty terms,

$$f = \frac{\dot{m}_c}{\dot{m}_c(\text{ref})} + \exp(\alpha T^*) + \exp(\beta \Delta T^*)$$
$$T^* = \frac{T_{\text{mean}} - T_{\max}}{T_{\max}}, \quad \Delta T^* = \frac{\Delta T - \Delta T_{\max}}{\Delta T_{\max}} \tag{1}$$
$$T_{\text{mean}} = \frac{1}{l_d}\int T \mathrm{d}x$$

and the mathematical notation can be written as $\arg\min_{D,S} f$, subject to bounds of D and S, where arg is a mathematical notation that represents the value of the argument D and S in their bounds that minimizes the cost function f.

In this description, $\dot{m}_c$ is the total coolant utilized, which is normalized by reference coolant level $\dot{m}_c(\text{ref})$. The soft average

temperature constraint on parameter T^* consists of the streamwise-averaged shell temperature (T_{mean}) and the maximum allowable blade temperature (T_{max}) that can be defined according to blade metal creep strength. The soft temperature gradient constraint on parameter ΔT^* is dependent on the difference between the maximum and the minimum wall temperatures (ΔT) and the maximum allowable temperature difference on the blade (ΔT_{max}), associated with the bearable thermal stresses. For the soft constraints, exponential terms are chosen since they are below one when constraints are within their limits (T^* and ΔT^* have negative values) and increase dramatically otherwise. α and β are weighting constants tuning the severity of these soft constraints. These constants control the objective function terms sensitivity (divergence rate) to an increase in T^* and ΔT^*. Such a formulation, as depicted in Eq. (1), enables utilizing an unconstrained algorithm which decreases convergence time.

The optimizer is based on a surrogate algorithm, which exists in MATLAB 2020B, and alternates between two phases—construction of surrogate and search for minimum. The first phase evaluates the objective function at points that are taken from a quasi-random sequence, scaled, and shifted to remain within the bounds. Then, it constructs a surrogate by interpolating a radial basis function through these points. The second phase searches for a minimum by sampling random points and evaluates a merit function based on the surrogate value and their locations. The search process stops when all the points remain sufficiently close to each other.

The optimizer separately generates geometry distributions using a 5-point piecewise cubic Hermite interpolating polynomial for $D(x)$ and $S(x)$ for pressure and suction sides. The number of polynomial control points determines the number of design variables and thereby optimization convergence time. Leading edge point is shared for pressure side and suction side, resulting in nine design variables each for hole diameter distributions, $D(x)$, and for hole spacing distributions, $S(x)$. Taking the geometry variables as input, the reduced-order model converges on local heat flux distributions and implicitly on metal temperature. Then, the integral coolant mass flowrate and wall temperature distribution are used for evaluating the cost function given by Eq. (1) as a minimization objective. The entire optimization process is outlined in the flowchart of Fig. 10.

The scaled-down C3X blade geometry with 33.5 mm chord is considered to be the demonstrative airfoil profile. Initial shell stress analysis is conducted and showed that 0.4 mm thickness withstands the external pressure conditions in a typical micro-gas turbine (see Table 4). Hot gas inlet total temperature and pressure are set to be 808 K and 243.5 kPa, respectively, whereas the cold gas inlet total temperature and pressure are set to be 374 K and 246 kPa. The static pressure and the uncooled airfoil heat transfer coefficients are as charted in Fig. 4. The average outer blade temperature value of the reference case (605 K) is taken as the maximum allowable metal temperature (T_{max}), while 20 K is selected as the maximum allowable temperature difference within the blade (ΔT_{max}) in order to minimize the risk of cracks due to thermal stress [22]. Based on basic thermal stress calculations using Inconel Alloy 718, around 55 MPa stress may occur for $\Delta T =$ 20 K in case the expansion is restrained, which is small compared with yield strength of the material (typically more than 700 MPa) at workable temperatures. Although case-dependent, 20 K temperature variation is considered as the limit for low crack risk [23].

Lastly, 2% of the hot gas mass flow is considered suitable for $\dot{m}_c(\text{ref}) = 1.1 \cdot 10^{-3}$ kg/s, and α, β are taken as 20 and 5, respectively. The latter are selected to achieve the same divergence rate of each exponential term for an increase in T_{mean} and ΔT.

In this example, a minimum of 50 μm hole diameter is chosen according to existing manufacturing technology limitations

Table 4 Structural analysis results for varying shell thickness

Shell thickness (mm)	Maximum equivalent stress (MPa)	Minimum safety factor
0.3	230.3	3.04
0.4	128.8	1.94
0.5	82.3	1.09

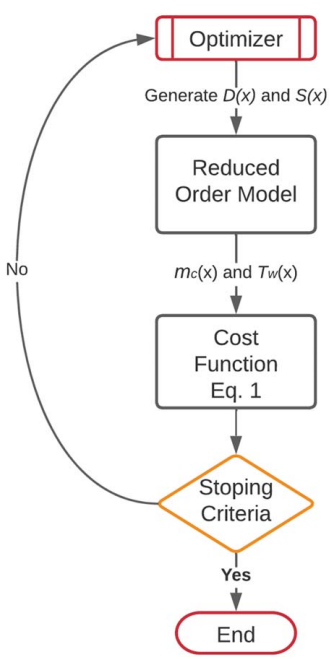

Fig. 10 Optimization flowchart

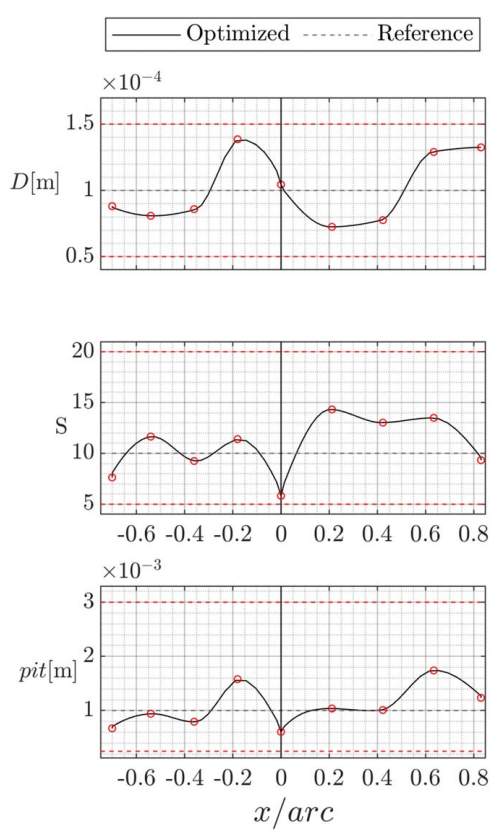

Fig. 11 Distributions of hole diameter, spacing, and pitch, in the optimized geometry (within the bounds of the optimized parameters) and the reference case from combined reduced-order model validation section with a constant of 0.1 mm cooling hole diameter at a constant pitch of 10

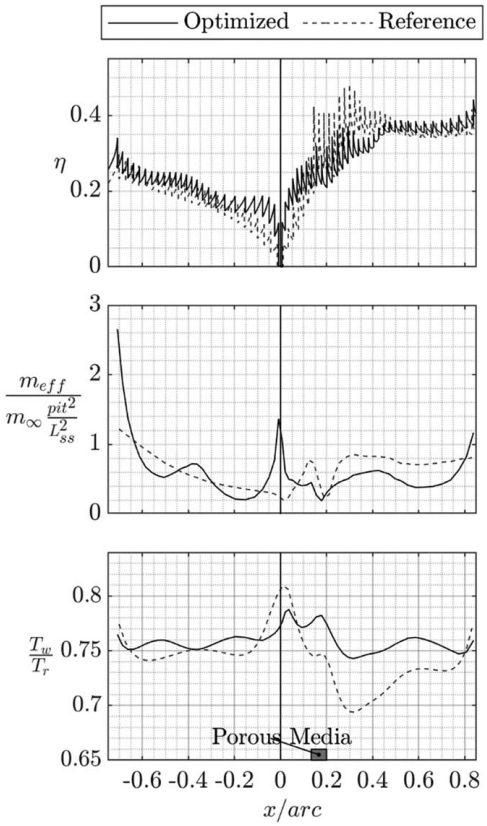

Fig. 12 Lateral-averaged adiabatic cooling effectiveness, coolant mass flowrates averaged over local hole pitch surface and wall temperature distributions for optimized effusion cooling hole and pitch according to Fig. 11 (T_r = 811 K)

[24,25]. In addition, very small spacing may reduce metal strength and therefore the limit is set to pit/$D = 5$. Circular holes at 90° injection angle are considered due to their relative ease of production. The holes are patterned as hexagonal arrays, thereby maximizing coolant wall coverage. Building upon these constraints, the final design variable bounds are $D(x) = [50 - 150]$ μm for hole diameter, and $S(x) = [5 - 20]$ for hole spacing.

Optimization Results. Based on the described framework, the optimized distributions of effusion-hole diameter and pitch are shown in Fig. 11. It is important to note that the solutions did not reach the bounds of the design variables. Contrasting the performance of the optimal effusion distribution, the reference benchmark case is considered with the constant 0.1 mm diameter effusion cooling holes at a pit/D of 10 (as analyzed in Combined Reduced-Order Model Validation section). For both cases, the corresponding lateral-averaged adiabatic effectiveness, coolant mass flowrates averaged over local hole pitch surface (normalized by the area surface around the hole—pit^2, providing a quantity equivalent to pitch-averaged-blowing ratio), and wall temperature distributions are shown in Fig. 12.

Expectedly, pitch-to-diameter ratio has a drastic effect on effectiveness, as it directly appears in the relevant correlation. The diameter dictates the coolant flowrate in the locality of the hole and the associated compound cooling effect. The optimal results show a general trend of maximizing effectiveness in the high wall temperature regions of the reference case. These regions include mainly the spikes in the leading edge and the trailing edge. In addition, modeling conduction through the shell greatly affects the streamwise wall temperature distribution, especially noticeable in the trailing edge region, where the wall temperature increases due to the uncooled metal piece. Near this area, S reduces (higher density) and D increases to compensate for the conducted heat from the uncooled trailing edge part. As a result, the overall temperature decreases at the trailing edge. For the leading edge, the reduced pitch (and S) for almost fixed D produces higher effectiveness, which minimizes the temperature spike in the leading edge. In the first half of the suction side (x/arc < 0.5), the optimal result has a lower D for the same pitch (higher S or lower density), which corresponds to lower amounts of coolant flow and effectiveness, therefore eliminating the too low temperature region. In conclusion, the resultant wall temperature distribution across the vane is more uniform than the reference case and varies only within the cost function limits, while the integral coolant mass flowrate consumption of the optimized effusion cooled blade is 1.66% of the mainstream flow, a 17% reduction from the reference case.

Summary and Conclusions

A conjugate reduced-order model, with internal boundary layer flow and nonuniform metal temperatures, is designed for skin cooling of turbine airfoils by single-wall effusion, and implemented as a preliminary design tool. Part I paper of this work comprehensively presents the development of the equations and numerical and experimental validations of its modules on several test cases. In this Part II, the validation of the complete conjugate model is conducted on coupled internal-effusion cooling of an entire turbine vane having a uniform diameter and pitch, subjected to transonic external flows. It is demonstrated that the reduced-order model adequately captures the physics of a fully conjugate aerothermal CFD simulation at five orders of magnitude smaller computational cost. Qualitatively, the predicted trends agree well with the full CFD results for film cooling effectiveness, heat transfer coefficient, and wall temperature. Quantitatively, effectiveness is predicted within a maximum 14% error near the leading edge and 4–8% elsewhere. The heat transfer coefficient (with film and conduction) is predicted within a maximum 17% error (as low as 3% at some regions). The maximum error reduces to 16% for film cooled-adiabatic heat transfer coefficient. For the wall temperature, the maximum error is 1.8%. Considering the complex nature of the problem (coolant distribution to suction and pressure sides from a single supply, coolant distribution between the holes, metal shell quasi-2D temperature field, and external film coverage), the developed method can be considered successful.

Then, the main utility of this low-fidelity tool is highlighted through integration into an optimization framework. An exemplary optimization of hole diameter and spacing distributions is conducted for designing a shell geometry subjected to representative mainstream Reynolds number of 87,780 ($3 \cdot 10^5$ based on exit velocity) and mainstream exit Mach number of $M = 0.9$. The objective is to minimize coolant flow while maintaining soft constraints on the variation and peak value of shell metal temperature. Compared to the reference case of fixed diameter and pitch, the resultant wall temperature distribution appears to be more uniform, while the integral coolant mass flowrate consumption is reduced by 17%. As the numerical optimization reduces the calculation load by limiting the number of time-consuming CFD simulations, it results in an efficient modeling tool for geometry generation and shape optimization. The outcome of this work is intended to provide the basis for the future development of single-wall effusion cooling technology in skin-cooled turbine airfoils.

Acknowledgment

The authors acknowledge the financial support of Minerva Research Center for Micro Turbine Powered Energy Systems (Max Planck Society Contract AZ5746940764).

Conflict of Interest

There are no conflicts of interest.

Data Availability Statement

The datasets generated and supporting the findings of this article are obtainable from the corresponding author upon reasonable request.

Nomenclature

f = friction coefficient or cost function
t = internal passage height (m)
u = velocity (m s^{-1})
x = curve-linear or streamwise direction (mm)
$\dot{m}$ = mass flowrate (kg s^{-1})
D = hole diameter (mm)
I = momentum flux ratio
M = Mach number or blowing ratio
P = pressure (Pa)
S = pitch-to-diameter ratio
T = temperature (K)
d_s = shell thickness (mm)
l_d = domain length (mm)
A_{act} = effective-hole area (m^2)
T_U = turbulence intensity
h,H = convection coefficient (W m^{-2} K^{-1})
Gz = Graetz number
Re = Reynolds number
arc = arc length of pressure or suction sides between leading and trailing edges
pit = holes pitch (mm)
η = lateral-averaged adiabatic cooling effectiveness

Abbreviations

CFD = computational fluid dynamics
CHT = conjugate heat transfer
ECM = electrochemical machining
EDM = electrical discharge machining
LR = low Reynolds number model
ML = Menter–Lechner model
RANS = Reynolds-averaged Navier–Stokes
ROM = reduced-order model
SC3X = scaled-down C3X blade
SST = shear stress transport
TIT = turbine inlet temperature (K)

Subscripts and Superscripts

c = coolant
f = with cooling
r = reference value
w = shell (or blade/vane) outer surface
eo = effusion-holes outlet
ps = pressure side
ss = suction side
s,S = static conditions
t,T = total/stagnation conditions
eff = effusion
w-in = shell inner surface
w-avg = shell center
0 = no cooling/stagnation conditions
1,2 = mainstream inlet and outlet, respectively

Appendix: Discussion on Manufacturing of Effusion Cooled Turbine Vanes/Blades

Addressing some of the challenges of moving into micro-cooling other works consider a blade structured from an effusive shell and a casted solid core also called skin cooling [1]. For validating the developed model through experiments and implementing such a design structural and manufacturing considerations should be examined. This configuration enables high mechanical strength while providing the versatility toward optimization of the coolant distribution. However, predicting the exact lateral-averaged adiabatic effectiveness remains a challenging task due to many influencing parameters (lateral spacing downstream distance blowing ratio density ratio main flow acceleration and hole shape). Guided by the results of this low-fidelity numerical model an iterative test-aided design approach can be considered through employing different shell geometries on the same casted core. This approach offers a potential to decouple turbine aerodynamics which dictate the core from the thermal management provided by the shell. Therefore, as the shell and core manufacturing processes are separated the design timeline and development costs of the turbine stage can be also reduced.

Comprising of a shell and a casted core the outline of the current blade topology is shown in Fig. 13. For micro-hole machining of the shell the three main methods that exist in the market are laser drilling electrical discharge machining (EDM) and electrochemical machining (ECM). Both laser drilling and EDM are very common in larger-scale cooling hole manufacturing [22,23] although the attainable surface roughness is relatively high with the potential for recast layer and micro-cracks. Therefore, post-processing may be necessary. Nevertheless, laser drilling appears to be the best available solution for effusion/skin cooling considering its speed of production and a large number of holes necessary. Once micro-drilling of the sheet metal is complete the surface can be bent according to the shape of the blade and welded together with the core.

In order to structurally strengthen the shell surface ribs can be added to the core. In this case, two intermediate ribs are considered along the span of the SC3X blade. Toward minimizing the shell thickness which improves manufacturability (including bending) and reduces coolant pressure drop static structural finite element

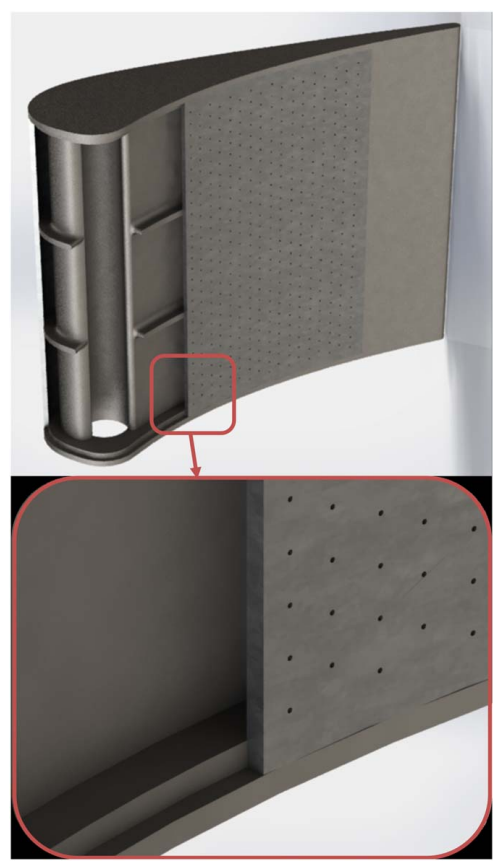

Fig. 13 Hypothetical effusion (skin) cooled SC3X vane/blade structure

analysis is performed on the external surface defining the sheet metal thickness as a parameter. The boundary conditions for this problem are fixed supports at the hub at the tip and at the trailing edge; frictional supports at the ribs; and a pressure difference of 600 kPa on the free surface. Maximum equivalent stress and minimum safety factor (based on stainless steel properties) are shown in Table 4.

References

[1] Bunker, R. S., 2013, "Gas Turbine Cooling: Moving From Macro to Micro Cooling," Proceedings of the ASME Turbo Expo 2013: Turbine Technical Conference and Exposition, San Antonio, TX, June 3–7, pp. 1–17.

[2] Polezhaev, J., 1997, "The Transpiration Cooling for Blades of High Temperatures Gas Turbine," Energy Convers. Manage., **38**(10–13), pp. 13–10.

[3] Eckert, E. R. G., and Cho, H. H., 1994, "Transition From Transpiration to Film Cooling," Int. J. Heat Mass Transfer, **37**(1), pp. 3–8.

[4] Selzer, B. M., Schweikert, S., Wolfersdorf, J., and Hald, H., 2012, "Transpiration Cooling Models Applied to Rocket Combustion Chambers," SFB/TRR40 Annual Report 2012.

[5] Cerri, G., Giovannelli, A., Battisti, L., and Fedrizzi, R., 2007, "Advances in Effusive Cooling Techniques of Gas Turbines," Appl. Therm. Eng., **27**(4), pp. 692–698.

[6] Krewinkel, R., 2013, "A Review of Gas Turbine Effusion Cooling Studies," Int. J. Heat Mass Transfer, **66**, pp. 706–722.

[7] Ligrani, P., Click, A., Ritchie, D., Liberatore, F., Patel, R., and Ho, Y. H., 2020, "Double Wall Cooling of an Effusion Plate With Cross Flow and Impingement Jet Combination Internal Cooling: Comparisons of Main Flow Contraction Ratio Effects," Int. J. Heat Mass Transfer, **150**, p. 119196.

[8] Kim, M., Shin, D. H., Kim, J. S., Lee, B. J., and Lee, J., 2021, "Experimental Investigation of Effusion and Transpiration Air Cooling for Single Turbine Blade," Appl. Therm. Eng., **182**, p. 116156.

[9] Murray, A. V., Ireland, P. T., and Rawlinson, A. J., 2017, "An Integrated Conjugate Computational Approach for Evaluating the Aerothermal and Thermomechanical Performance of Double-Wall Effusion Cooled Systems," Proceedings of the ASME Turbo Expo 2017: Turbomachinery Technical Conference and Exposition, Charlotte, NC, June 26–30, pp. 1–12.

[10] Ngetich, G. C., Murray, A. V., Ireland, P. T., and Romero, E., 2019, "A Three-Dimensional Conjugate Approach for Analyzing a Double-Walled Effusion-Cooled Turbine Blade," ASME J. Turbomach., **141**(1), p. 011002.

[11] Goldstein, R. J., 1971, "Film Cooling," Adv. Heat Transfer, **7**, pp. 321–379.

[12] Sellers, J. P., 1963, "Gaseous Film Cooling With Multiple Injection Stations," AIAA J., **1**(9), pp. 2154–2156.

[13] Murray, A. V., Ireland, P. T., Wong, T. H., Tang, S. W., and Rawlinson, A. J., 2017, "High Resolution Experimental and Computational Methods for Modelling Multiple Row Effusion Cooling Performance," 12th European Conference on Turbomachinery Fluid Dynamics and Thermodynamics, ETC 2017, Stockholm, Sweden, Apr. 3–7

[14] Murray, A. V., Ireland, P. T., and Romero, E., 2019, "Experimental and Computational Methods for the Evaluation of Double-Wall, Effusion Cooling Systems," Proceedings of the ASME Turbo Expo 2019: Turbomachinery Technical Conference and Exposition, Phoenix, AZ, June 17–21, pp. 1–16.

[15] Elmukashfi, E., Murray, A. V., Ireland, P. T., and Cocks, A. C. F., 2020, "Analysis of the Thermomechanical Stresses in Double-Wall Effusion Cooled Systems," ASME J. Turbomach., **142**(5), p. 051002.

[16] Murray, A. V., Ireland, P. T., and Romero, E., 2020, "An Experimentally Validated Low Order Model of the Thermal Response of Double-Wall Effusion Cooling Systems for HP Turbine Blades," Proceedings of the ASME Turbo Expo 2020: Turbomachinery Technical Conference and Exposition, Virtual, Sept. 21–25, pp. 1–13.

[17] Hylton, L. D., Mihelc, M. S., Turner, E. R., Nealy, D. A., and York, R. E., 1983, "Analytical and Experimental Evaluation of the Heat Transfer Distribution Over the Surfaces of Turbine Vanes," NASA Report 19830020105.

[18] Wlassow, F., Duchaine, F., Leroy, G., and Gourdain, N., 2010, "3D Simulation of Coupled Fluid Flow and Solid Heat Conduction for the Calculation of Blade Wall Temperature in a Turbine Stage," Proceedings of the ASME Turbo Expo 2010: Power for Land, Sea, and Air, Glasgow, UK, June 14–18, pp. 1–12.

[19] Bak, J. G., Cho, J., Lee, S., and Kang, Y. S., 2016, "Effects of Inlet Turbulence Conditions and Near-Wall Treatment Methods on Heat Transfer Prediction Over Gas Turbine Vanes," Int. J. Aeronaut. Space Sci., **17**(1), pp. 8–19.

[20] Metzger, D. E., Takeuchi, D. I., and Keunstler, P. A., 1973, "Effectiveness and Heat Transfer With Full-Coverage Film Cooling," ASME J. Eng. Power, **95**(3), pp. 180–184.

[21] Winka, J. R., Anderson, J. B., Boyd, E. J., Bogard, D. G., and Crawford, M. E., 2014, "Convex Curvature Effects on Film Cooling Adiabatic Effectiveness," ASME J. Turbomach., **136**(6), p. 061015.

[22] Mazur, Z., Luna-Ramírez, A., Juárez-Islas, J. A., and Campos-Amezcua, A., 2005, "Failure Analysis of a Gas Turbine Blade Made of Inconel 738LC Alloy," Eng. Fail. Anal., **12**(3), pp. 474–486.

[23] Sadowski, T., and Golewski, P., 2011, "Multidisciplinary Analysis of the Operational Temperature Increase of Turbine Blades in Combustion Engines by Application of the Ceramic Thermal Barrier Coatings (TBC)," Comput. Mater. Sci., **50**(4), pp. 1326–1335.

[24] Hasan, M., Zhao, J., and Jiang, Z., 2017, "A Review of Modern Advancements in Micro Drilling Techniques," J. Manuf. Process., **29**, pp. 343–375.

[25] Imran, M., Mativenga, P. T., Gholinia, A., and Withers, P. J., 2015, "Assessment of Surface Integrity of Ni Superalloy After Electrical-Discharge, Laser and Mechanical Micro-Drilling Processes," Int. J. Adv. Manuf. Technol., **79**(5–8), pp. 1303–1311.